PNAS
www.pnas.org

Supplementary Information for

Mapping temperature-dependent conformational change in the voltage-sensing domain of an engineered heat-activated K^+ channel.

Hongbo Chen[1, 2], Jiahua Deng [3], Qiang Cui [3], Baron Chanda [1, 4, *], Katherine Henzler-Wildman[1,2, *]

* Corresponding authors Katherine Henzler-Wildman, Baron Chanda
Email: henzlerwildm@wisc.edu, bchanda@wustl.edu.

This PDF file includes:

Figures S1 to S11

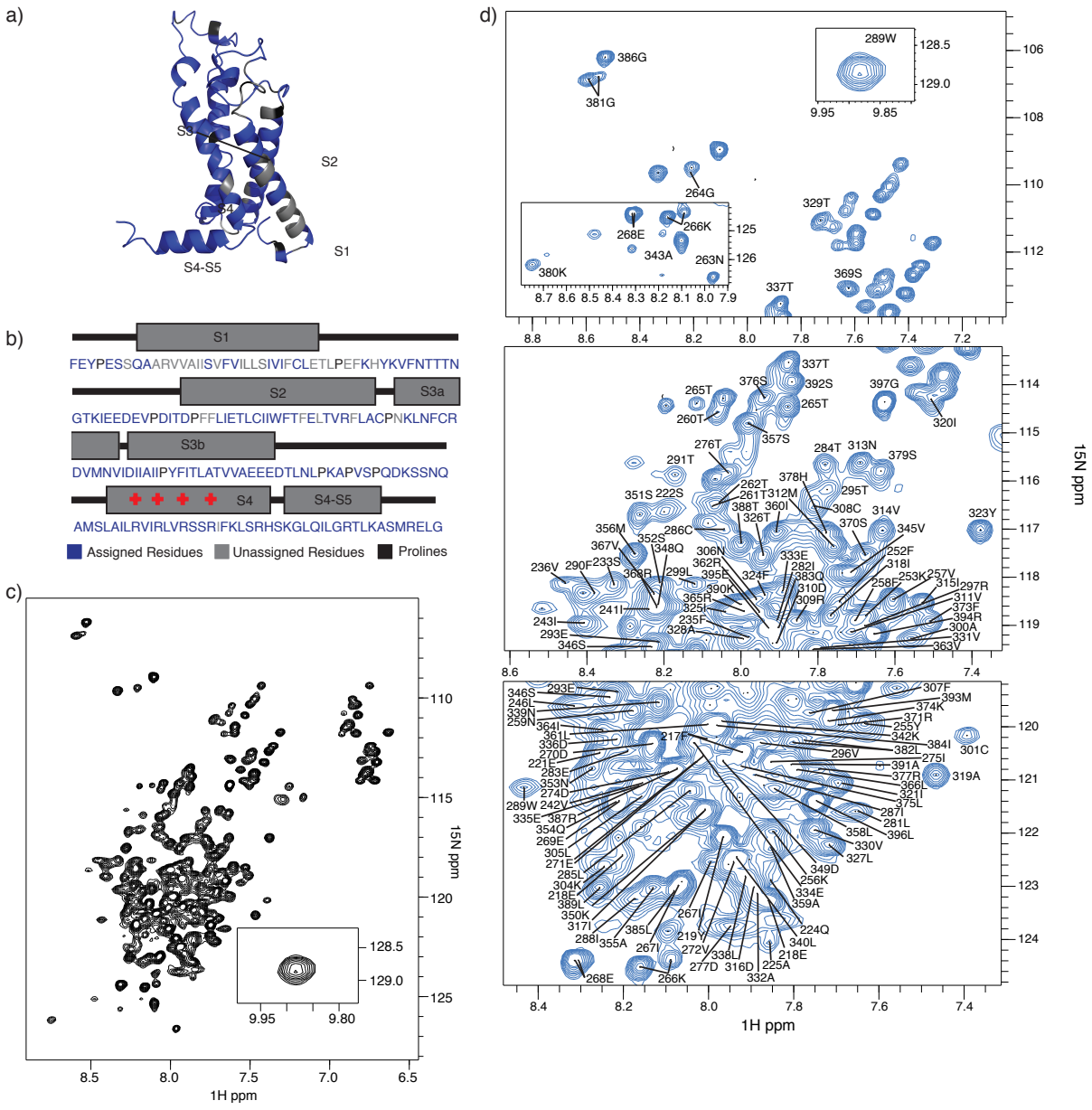

Figure S1. TS-VSD construct and NMR assignment. (a) Homology model and (b) amino acid sequence of the isolated Shaker-VSD (217-397), which spans from the S1 transmembrane helix to the S4-S5 linker. Residues with assigned backbone resonances are colored blue. Prolines are colored black and unassigned non-proline residues are colored grey. (c) ^{1}H-^{15}N TROSY-HSQC NMR spectrum of the TS-VSD construct in 1.6% LPPG micelles at pH 7.0 and 45°C. (d) An enlarged view of the spectrum with chemical shift assignments.

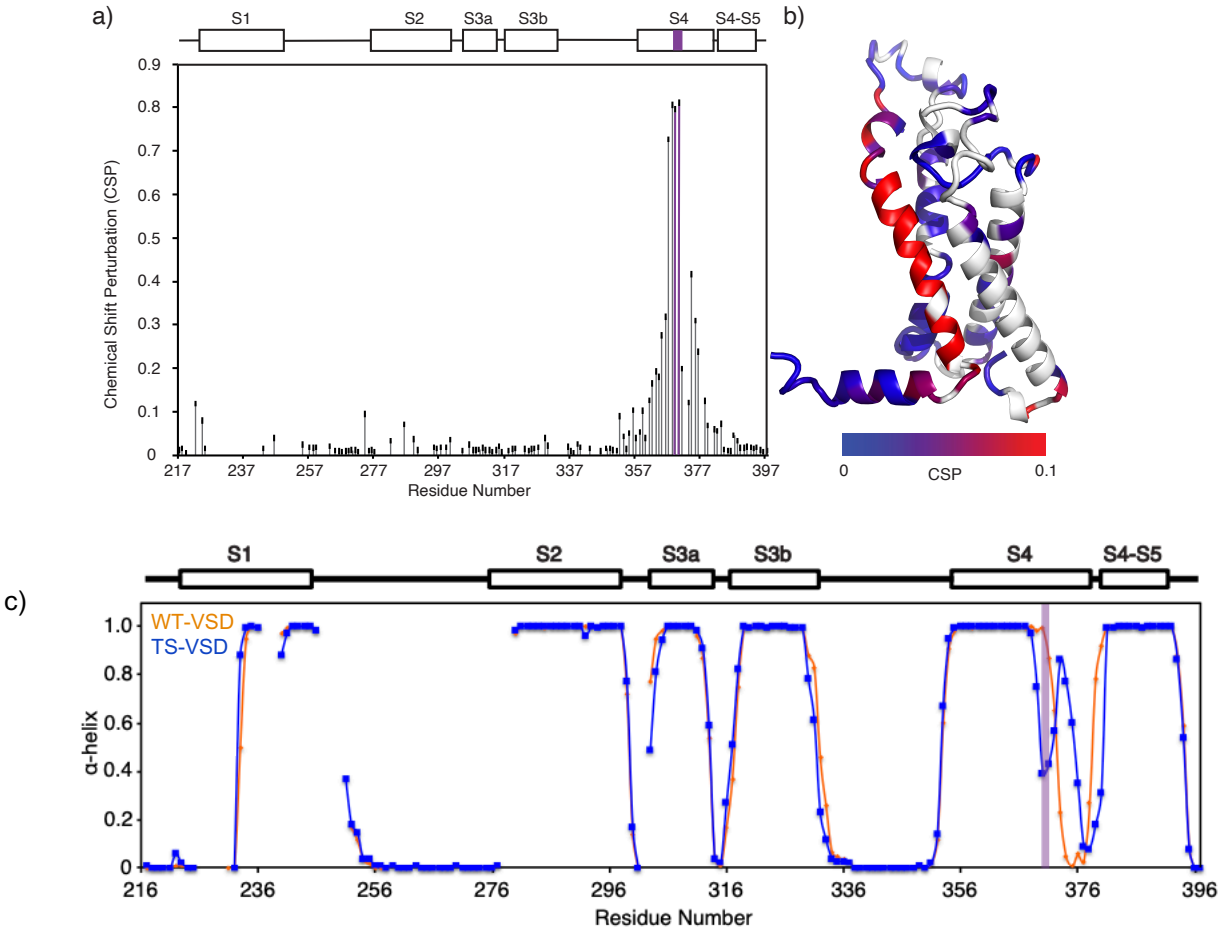

Figure S2. Chemical shift perturbation and secondary structure changes induced by the S2bot mutation is the same at 28 °C. (a) The chemical shift perturbation (CSP) between WT-VD and TS-VSD at 28 °C is essentially the same as observed at 45 °C. CSP was calculated as from the 3D-HNCO spectra at 28°C and numbering is as in Figure 2. Sequence coverage is slightly reduced due to reduced resolution at the lower temperature. (b) The CSP distribution is mapped on the homology model of isolated Shaker-VSD with a blue to red color scale. Unassigned residues are shown in white. Significant CSP ≥ 0.1 (red) is observed at the site of mutation and extending along the S4 transmembrane helix and into the adjoining loops. (c) The α-helical propensity of WT-VSD (orange) and TS-VSD (blue) calculated using PECAN (*61*) instead of TALOS+ (*25*) for analysis of the backbone NMR chemical shifts (H_N, N, Co, Cα and Cβ) yields nearly identical results, showing the S2bot mutation alters the structure of the S4 helix.

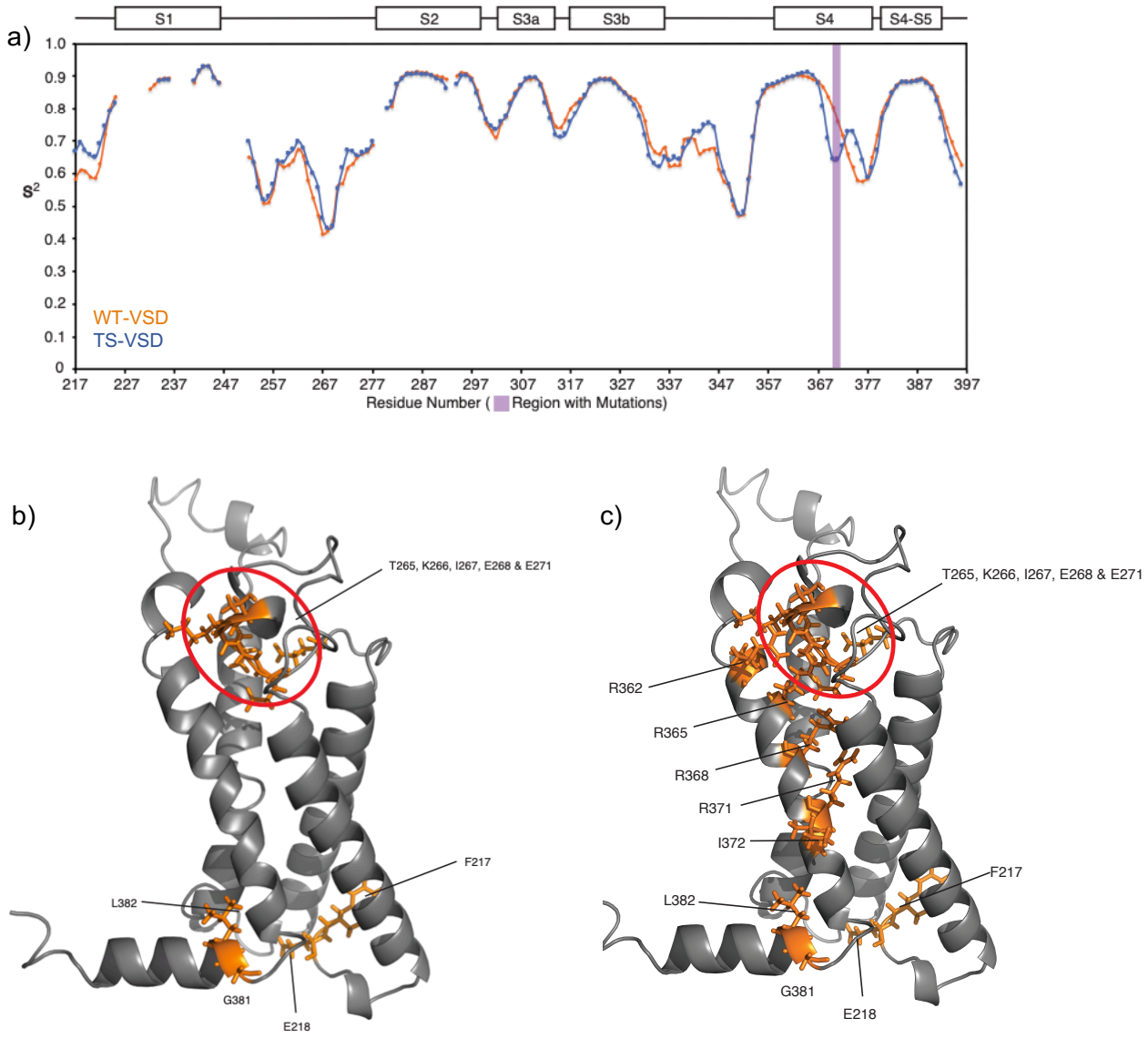

Figure S3. Effect of S2bot mutation on isolated VSD dynamics and flexibility. (a) The order parameter (S^2) profiles predicted for WT-VSD (orange) and TS-VSD (blue) based on analysis of the backbone chemical shifts (*25*) are shown with numbering according to the full-length Shaker sequence (secondary structure illustrated above the graph). The position of V369 and F370 in WT, which are mutated to serines in S2bot, is highlighted in purple. The reduction in order parameter observed in the C-terminal half of the S4 helix indicates the S2bot serine mutations may increase ps-ns flexibility in this region. Residues of TS-VSD (b) and WT-VSD (c) exhibiting peak doubling in the well-resolved 3D TROSY-HNCO or TROSY-HNCA NMR spectra for TS-VSD are highlighted in orange. Unlike our prior study of WT-VSD (24), peak doubling is not observed within the S4 transmembrane helix in TS-VSD.

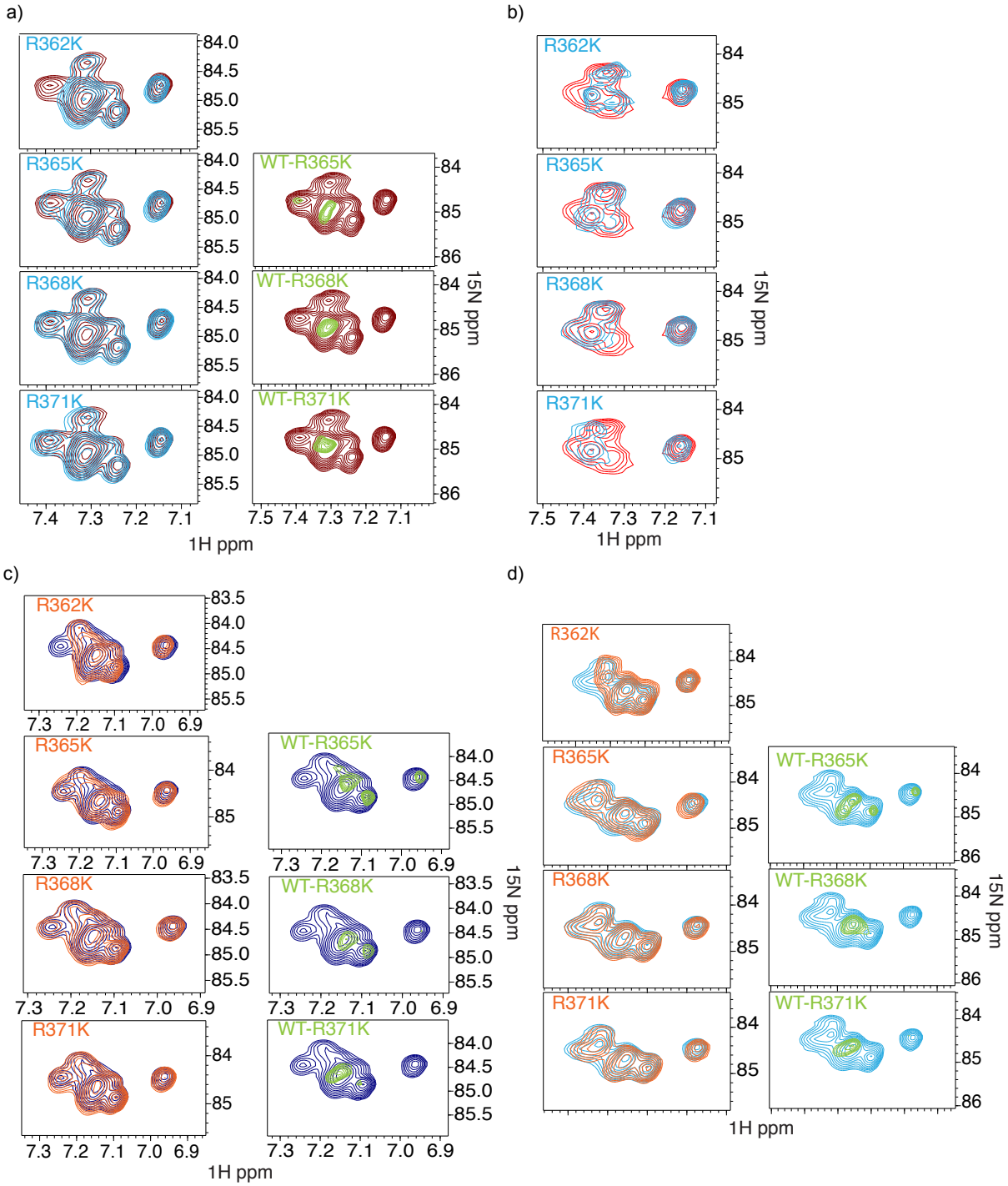
a)
R362K
R365K
R368K
R371K
WT-R365K
WT-R368K
WT-R371K
15N ppm
1H ppm
b)
R362K
R365K
R368K
R371K
15N ppm
1H ppm
c)
R362K
R365K
R368K
R371K
WT-R365K
WT-R368K
WT-R371K
15N ppm
1H ppm
d)
R362K
R365K
R368K
R371K
WT-R365K
WT-R368K
WT-R371K
15N ppm
1H ppm

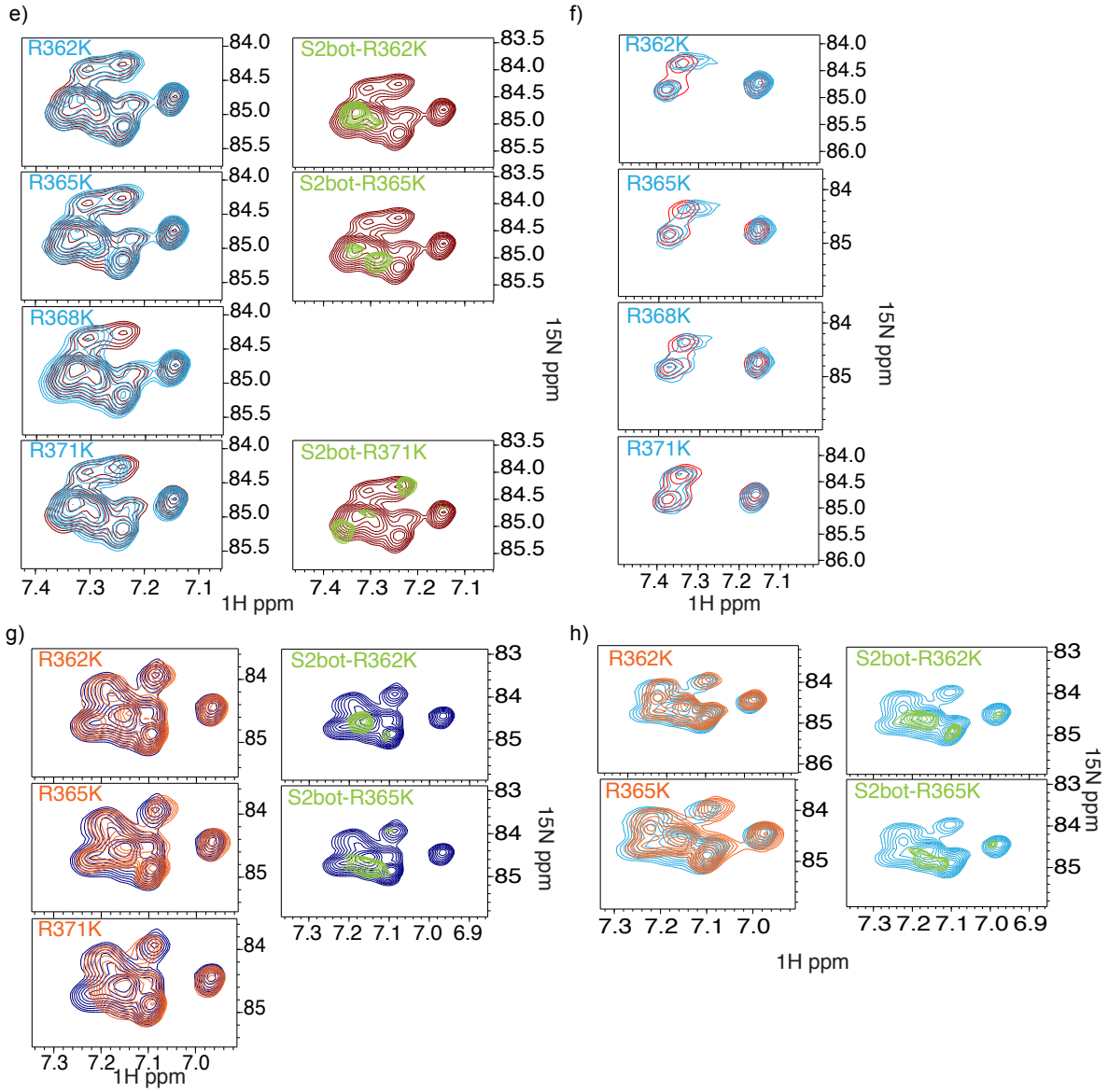

Figure S4. Sequence specific assignment of arginine sidechains through site-specific R to K mutation. Overlay of the HεNε region of the ^{15}N-^{1}H TROSY-HSQC spectra for the VSD and a R to K mutation (left side of each panel), as well as the overlay with the difference spectrum (right side) for assignments in crowded regions. (a) WT-VSD at pH 7.0 and 28°C. WT-VSD (dark red), R-to-K mutant (blue), difference (green). The arginine resonance is assigned to the strongest peak in the difference spectrum with any minor peaks attributed to chemical shift changes in other resonances induced by proximity to the mutation. (b) WT-VSD at pH 7.7 and 28°C. WT-VSD (red), R-to-K mutant (light blue). There are clear differences between the original and R to K mutant spectra, indicating that the voltage dependent S4 arginines are not exchange broadened and the peaks in the spectrum that have broadened at pH 7.7 must be from arginine residues in the more exposed loop regions. (c) WT-VSD at pH 7.0 and 8°C. WT-VSD (dark blue), R-to-K mutant (orange), difference spectrum (green). (d) WT-VSD at pH 7.7 and 8°C. WT-VSD (light blue), R-to-K mutant (orange), difference spectrum (green). resonances induced by the mutation. (e) TS-VSD at pH 7.0 and 28°C. TS-VSD (dark red), R-to-K mutant (blue), difference (green). (f) TS-VSD at pH 7.7 and 28°C. TS-VSD (red), R-to-K mutant (light blue), difference (green). There is a profound loss of arginine HeNe signals between (e) and (f), and there is little (R362K) to no change in the intensity of the peaks that are observed upon R to K mutation of the S4 arginines, unambiguously indicating that R365, R358, and R371 are not visible in the TS-VSD spectrum due to significantly increased hydrogen exchange with water. (g) TS-VSD at pH 7.0 and 8°C. TS-VSD (dark blue), R-to-K mutant (orange), difference (green). (h) TS-VSD at pH 7.7 and 8°C. TS-VSD (light blue), R-

to-K mutant (orange), difference (green). Note that our backbone chemical shift analysis indicated structural changes and enhanced flexibility in the lower portion of S4 where these arginine residues are located. These side chains are highly dynamic, which is what enables us to observe them even at 8 °C where the backbone resonances are severely broadened. In this fast-exchange regime, increased dynamics would lead to further sharpening of the resonances, not the line broadening as we see here. Thus, the NMR data unambiguously indicates enhanced hydration of the S4 arginine residues at elevated temperatures in the TS-VSD but not the WT-VSD.

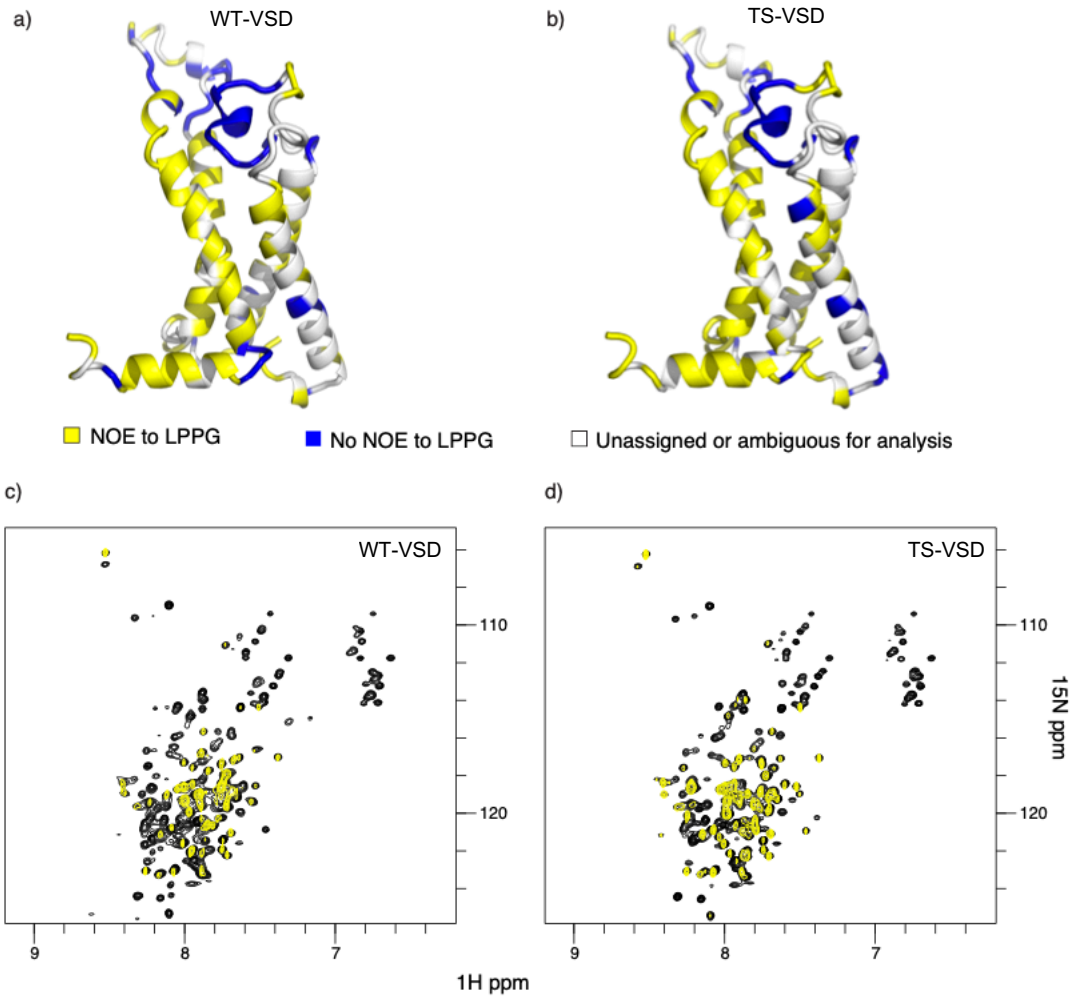

Figure S5. Both WT-VSD and TS-VSD remain stably embedded in the LPPG micelle. Residues within WT-VSD (a) and TS-VSD (b), with visible crosspeaks to the terminal methyl of LPPG in an ^{15}N-edited NOESY-TROSY experiment are yellow on the homology model of the Shaker-VSD. Residues without crosspeaks to LPPG are colored blue, and residues without assignments or peak overlap are colored grey. The raw data for WT-VSD (c) and TS-VSD (d) are shown below, with an overlay of the ^{15}N-^{1}H TROSY-HSQC spectrum (black) and the LPPG methyl plane (~1.24 ppm at 45°C) from the ^{15}N-edited NOESY-TROSY spectrum (yellow). Regions with NOESY crosspeaks to LPPG are nearly identical in WT-VSD and TS-VSD, and include nearly all resolved and assigned residues within the transmembrane helices. This indicates that the VSD is embedded in the LPPG micelle and the S2bot mutation does not alter this.

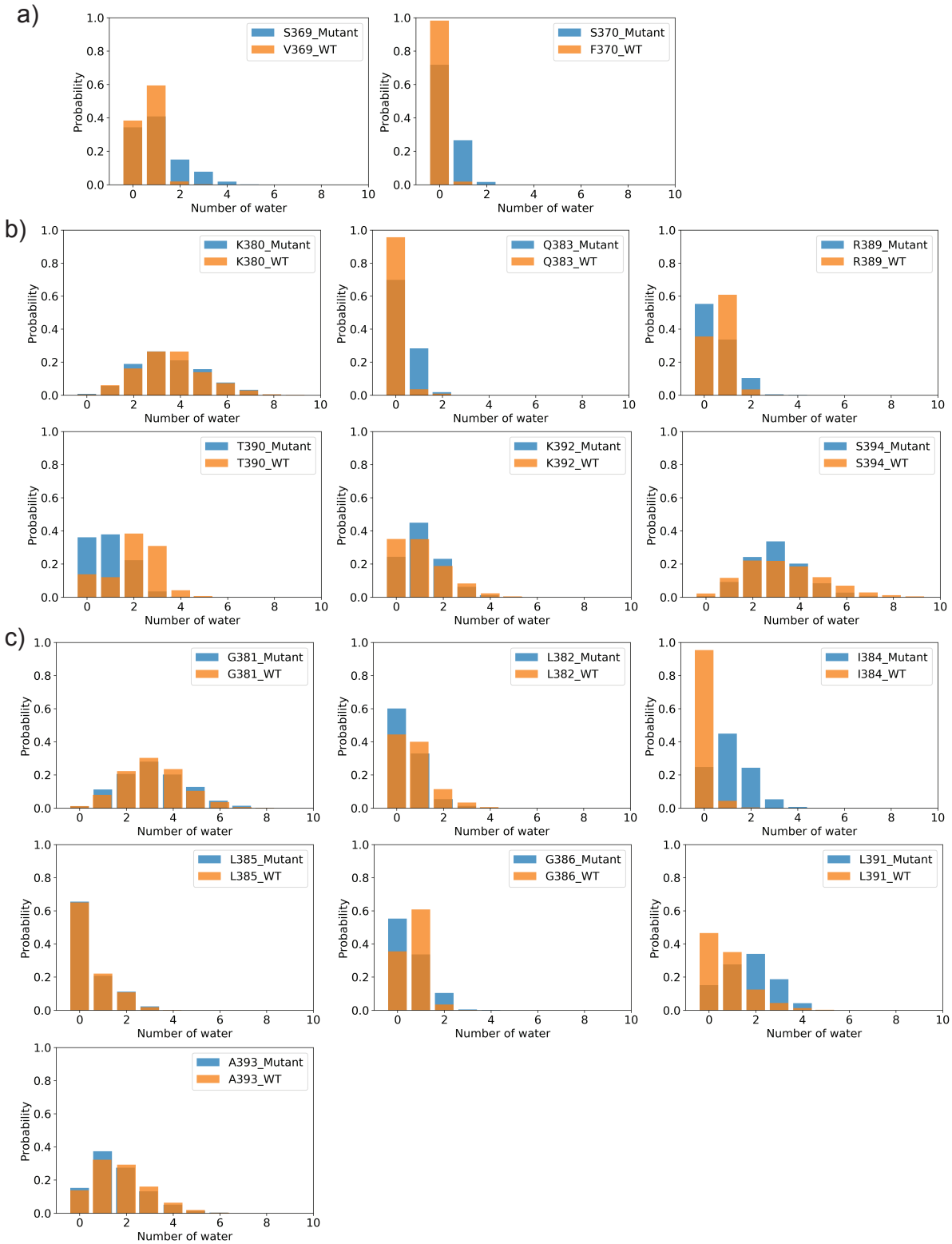

Figure S6. Histogram of the number of water molecules within 5 Å of the backbone N during the conventional MD simulations. (a) As expected, the TS-VSD$_{1.2}$ mutant features a higher level of hydration due to the increased polarity at the mutation sites. (b) Polar/charged residues and (c) nonpolar residues in the S4-S5 linker show a redistribution of water in this region.

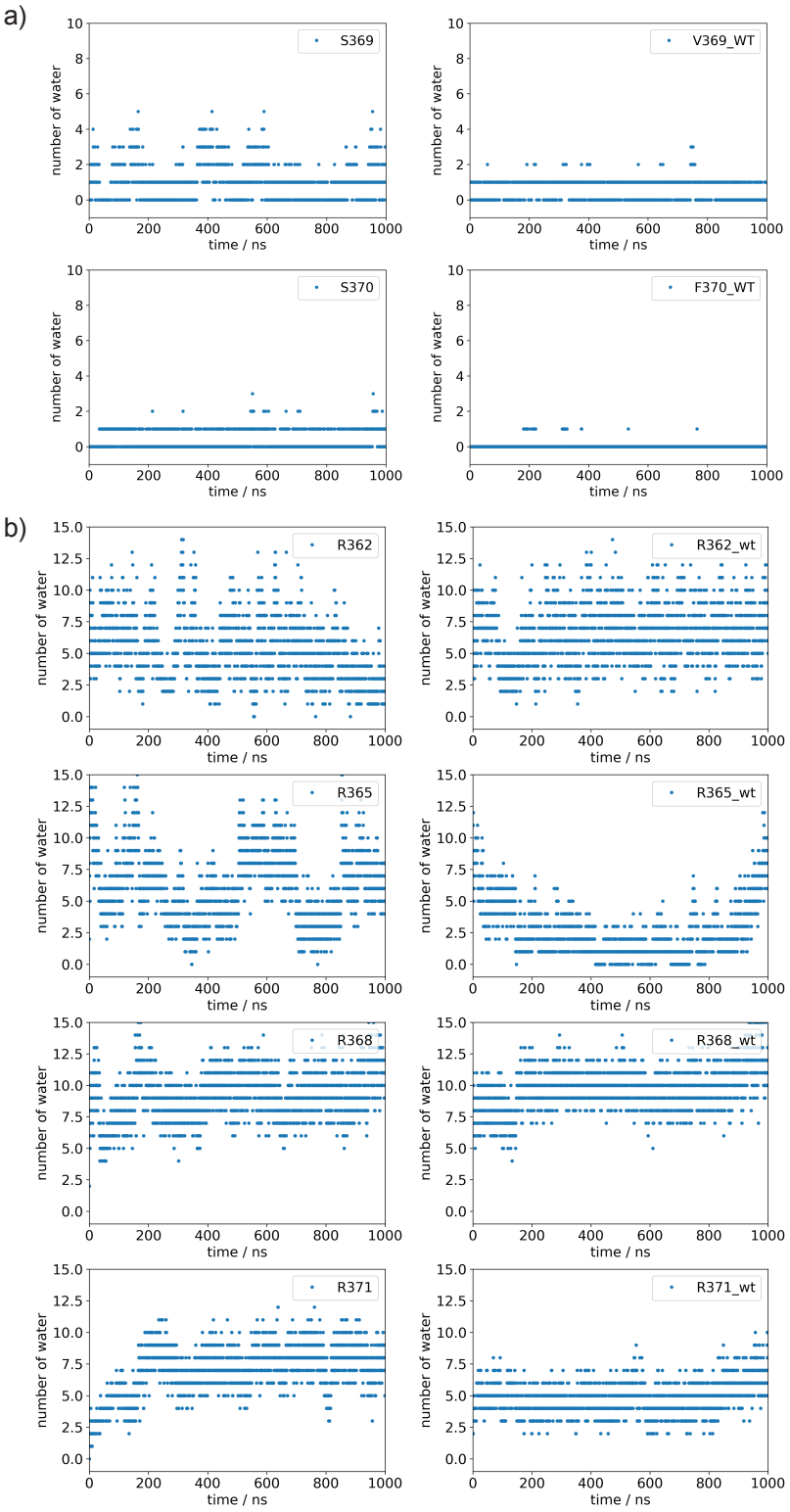

Figure S7. Time evolution of water molecules during the conventional MD simulations. (a) Within 5 Å of the backbone at the mutation sites (TS-$VSD_{1.2}$ on left, WT- $VSD_{1.2}$ on right) and (b) within 6 Å of Hε in the four voltage-sensing arginines (TS- $VSD_{1.2}$ on left, WT- $VSD_{1.2}$ on right).

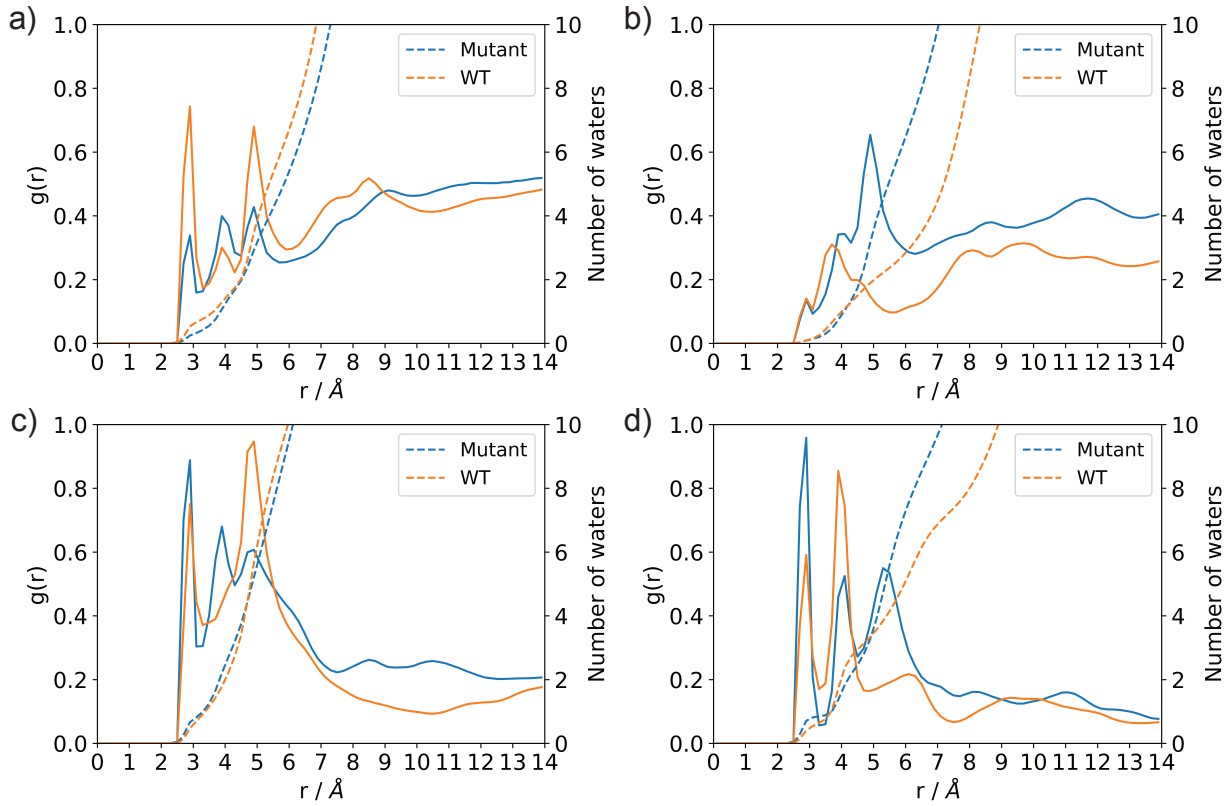

Figure S8. The radial distribution function (solid lines) and the cumulative distribution function (dash lines) of water molecules around Hε in the voltage-sensing arginines during the conventional MD simulations for TS-VSD$_{1.2}$ (blue) and WT-VSD$_{1.2}$ (orange). a) R362, b) R365, c) R368, and d) R371.

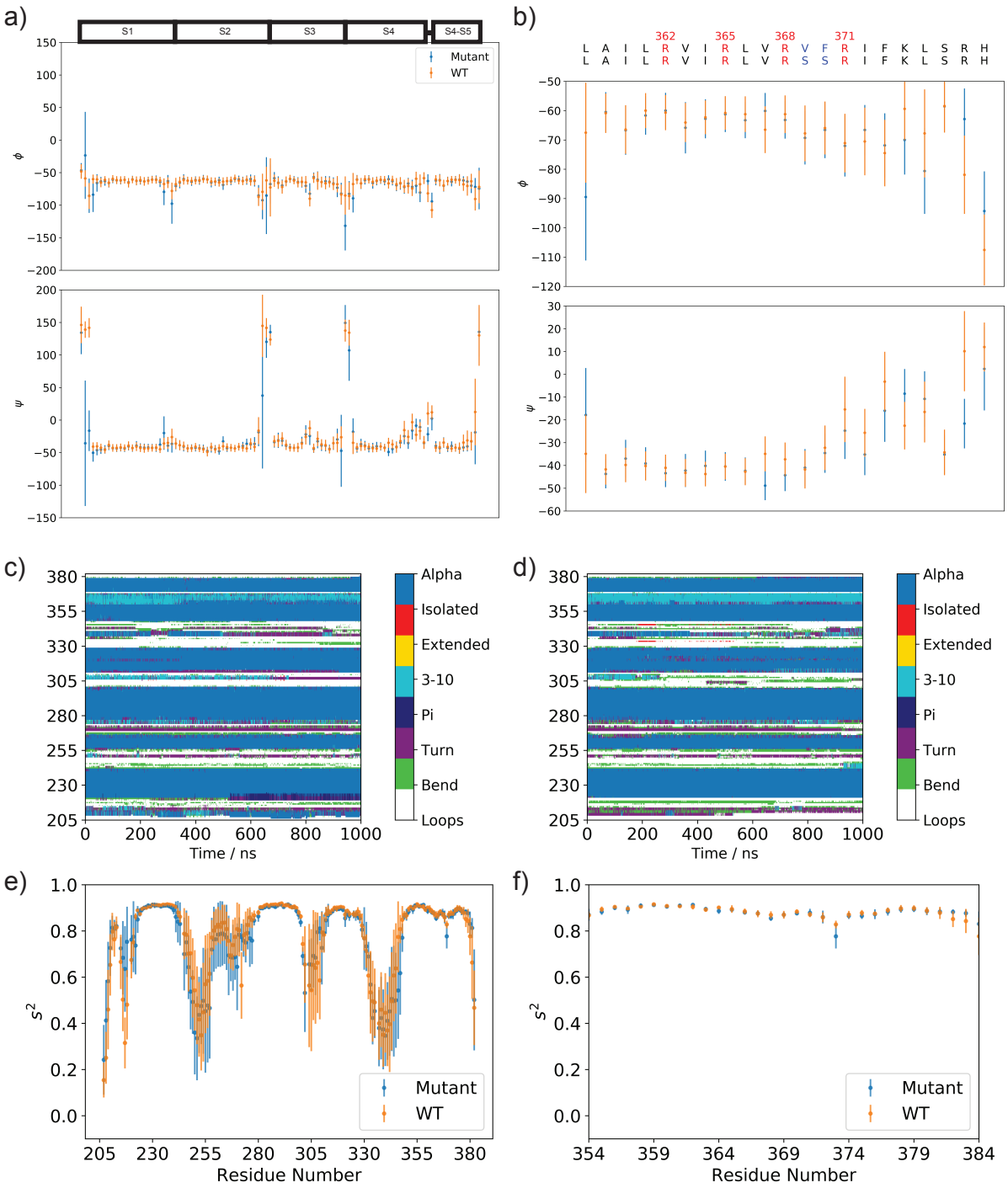

Figure S9. Backbone structure and dynamics calculated from 1 μs conventional MD simulations. Backbone ϕ and ψangles are shown for (a) all residues in the VSD and (b) residues in S4. No major structural change is observed between the WT-VSD$_{1.2}$ (orange) and the TS-VSD$_{1.2}$ (blue). Secondary structure fluctuations for (c) TS-VSD$_{1.2}$ and (d) WT-VSD$_{1.2}$. (e) Model-free order parameter, S^2, of backbone N-H computed by the equilibrium method based on 1 μs conventional MD simulations for all residues in the WT-VSD$_{1.2}$ (orange) and TS-VSD$_{1.2}$ (blue); (b) Order parameters of residues near the mutation sites. Error bars show the standard deviations from block average.

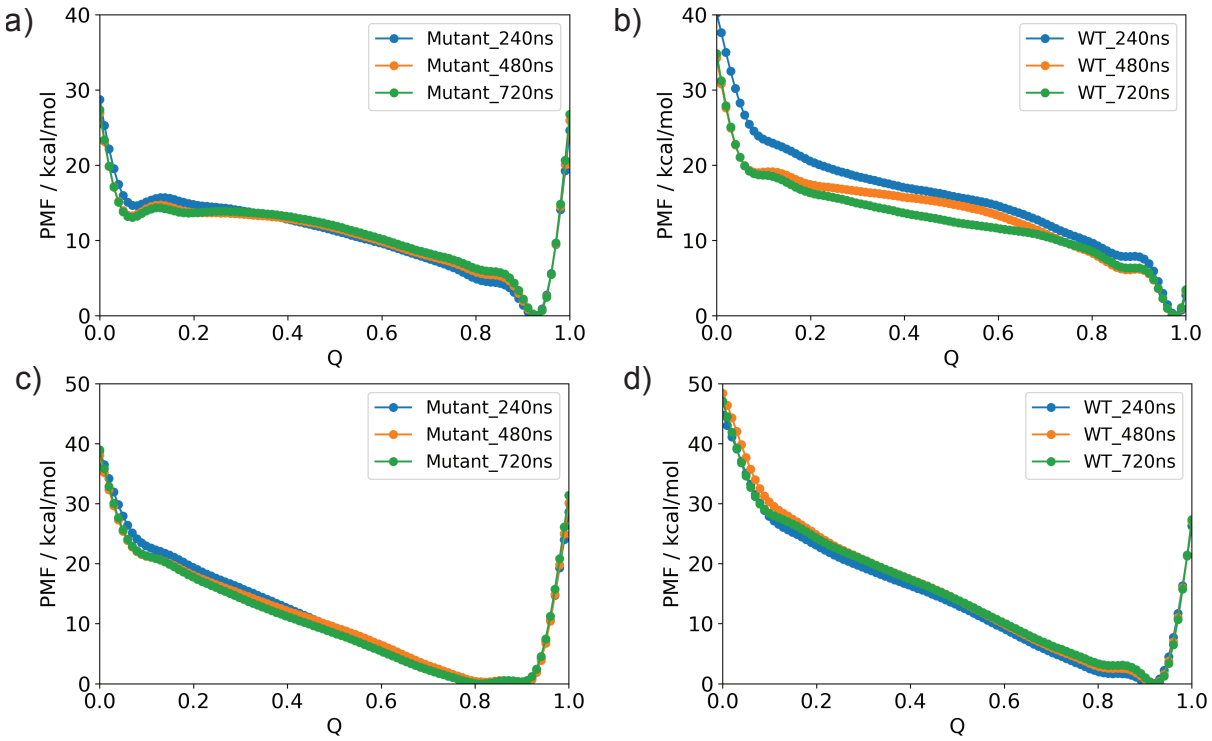

Figure S10. Convergence of the PMF from multiple-walker well-tempered metadynamics simulations (α-helix) are shown for (a) TS-VSD$_{1.2}$ and (b) WT-VSD$_{1.2}$. Convergence of the PMF from multiple-walker well-tempered metadynamics simulations (3_{10}-helix) are shown for (c) TS-VSD$_{1.2}$ and (d) WT-VSD$_{1.2}$.

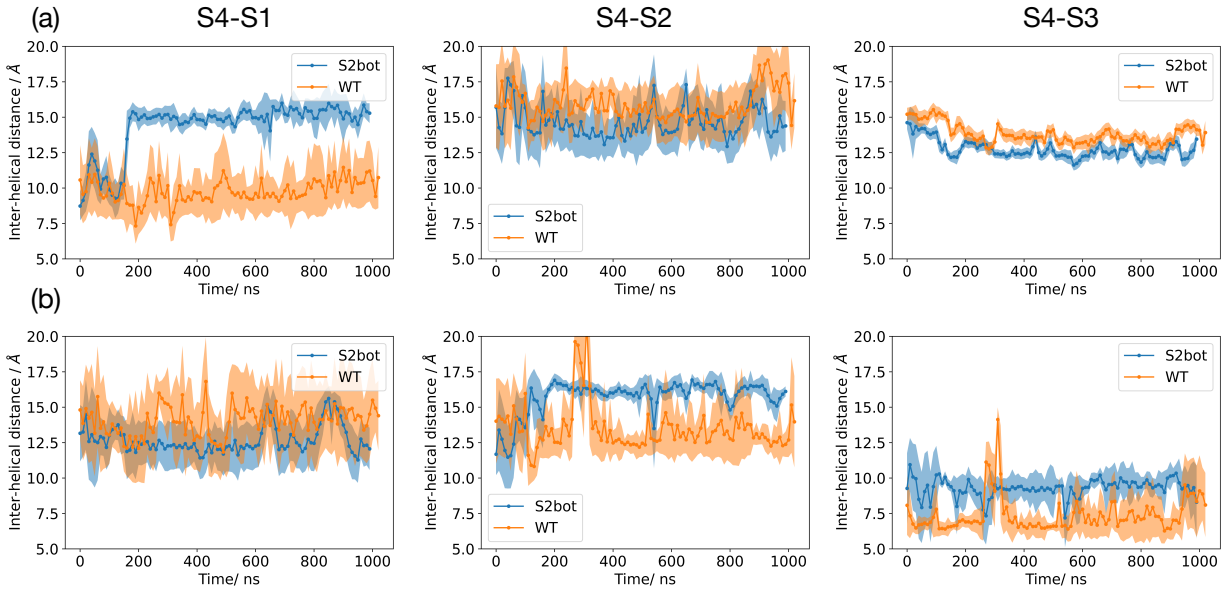

Figure S11. Average interhelical distances measured between the mutation site in S4 and helices S1, S2 and S3 during molecular dynamics simulations. Panel a is for residue 369, and panel b is for residue 370. For each plot, the distance is defined as the minimal distance between the center of mass (COM) of the mutation site and any residue's COM in the other helix. The plots show values averaged over 10 ns windows, and the shaded area indicates values within 1 standard deviation of the local average. The results illustrate the general trend that the packing of the helices becomes looser in the TS-VSD relative to the WT-VSD in the region near the mutation sites.